Infrared Limb-Darkening Effects for the Earth-Atmosphere System

S. K. Gupta*
NASA Langley Research Center, Hampton, Virginia
S. N. Tiwari† and C. S. Vemuru‡
Old Dominion University, Norfolk, Virginia
and
J. T. Suttles§
NASA Langley Research Center, Hampton, Virginia

An infrared radiative transfer model has been developed for evaluating anisotropic functions in the longwave region (5-50 μm) due to limb-darkening effects in the Earth's atmosphere. An accurate narrow-band model of absorption has been used for computing transmission functions of the atmosphere. Absorption due to all major and minor atmospheric constituents has been taken into account including the continuum absorption due to water vapor. Anisotropic functions have been calculated for several latitudinal and seasonal climatological-average model atmospheres. Many more radiosonde-measured atmospheric models representing a wide range of meteorological parameters have also been used in this study. The effects of the variability of various meteorological parameters, e.g., surface temperature, surface relative humidity, and cloud-top height have been examined. It has been found that the variability of cloud parameters has the largest effect on the infrared anisotropic functions.

Nomenclature

B_ν = Planck function
M = integrated flux density
M_ν = spectral flux density
$L(\theta)$ = integrated radiance
L_ν = spectral radiance
p_s = surface pressure
p_z = pressure at altitude z
$R(\theta)$ = anisotropic function
T_s = surface temperature
T_z = temperature at altitude z
w_s = mixing ratio at surface
w_z = mixing ratio at altitude z
z_c = cloud height
ϵ_c = cloud emissivity
ϵ_s = surface emissivity
θ = nadir viewing angle
λ = scale-height parameter
τ_ν = spectral transmittance

Subscripts

ν = frequency
s = surface
z = altitude z

Introduction

INFRARED radiant exitance at the top of the atmosphere is an important component of the radiation budget of the Earth-atmosphere system and is thus a valuable parameter for weather and climate studies.[1-3] Since satellite-borne instruments measure outgoing radiance in a certain direction, methods for estimating radiant exitance from these measurements are extremely important. As shown in Fig. 1, the dashed straight line represents outgoing radiance as a function of viewing zenith angle in the absence of any atmosphere while the solid curves represent the same for three climatological-average atmospheric models. It is clear that the presence of atmosphere imparts anisotropy to the outgoing radiance and makes the estimation of radiant exitance considerably more difficult compared to the isotropic radiance represented by the straight line.[4,5] It is also clear from Fig. 1 that the magnitude of anisotropy is different for different atmospheric conditions. Detailed knowledge of anisotropic functions (defined in the next section) of the atmosphere and effects of variability of atmospheric parameters on them is necessary for converting measured radiances to the meteorologically significant parameter, namely, radiant exitance at the top of the atmosphere, which is assumed to be 30 km for the present study.

A study of the anisotropic function in the atmosphere has assumed greater importance recently because of its desirability for the Earth radiation budget experiment. This experiment is designed to measure the radiation budget of the Earth-atmosphere system at the top of the atmosphere. The scanning radiometer which is an important component of the instrument complement measures the radiance emanating at the top in a given direction. These directional radiances can be converted to the total outgoing flux density only if the anisotropic functions for the atmosphere are known.

The present investigation was undertaken to study the effects of the variability of various meteorological parameters on the anisotropic functions. A number of climatological-average model atmospheres representing their latitudinal and seasonal variability over the entire globe have been used for computation of these functions. Several more radiosonde-measured atmospheric models covering a wide range of meteorological conditions have also been used.

Presented as Paper 83-0161 at the AIAA 21st Aerospace Sciences Meeting, Reno, Nev., Jan. 10-13, 1983; received Sept. 10, 1983; revision received April 12, 1984.

*NASA-NRC Resident Research Associate.
†Eminent Professor, Department of Mechanical Engineering and Mechanics. Associate Fellow AIAA.
‡Graduate Research Assistant, Department of Mechanical Engineering and Mechanics.
§Senior Research Scientist. Member AIAA.

Theory and Radiation Model

Upwelling spectral radiance at the top of the plane-parallel clear atmosphere in a direction θ relative to nadir is given by

$$L_\nu(\theta) = \epsilon_s B_\nu(T_s)\tau_{\nu s}(\theta) + \int_{\tau_{\nu h}}^{1} B_\nu(T_z)\,\mathrm{d}\tau_{\nu z}(\theta) \qquad (1)$$

where the first term on the right-hand side represents the radiation from the surface and the second term, the radiation from the atmosphere. Radiance for an overcast atmosphere is obtained from this equation by treating the cloud top as the underlying surface and considering only that part of the atmosphere which lies above the cloud. For partly cloudy conditions, the radiance is obtained as the cloud-fraction weighted sum of the overcast and clear radiances.

Integrated outgoing radiance $L(\theta)$ is obtained by integrating the spectral radiance as

$$L(\theta) = \int_{\Delta\nu} L_\nu(\theta)\,\mathrm{d}\nu \qquad (2)$$

The frequency range of interest $\Delta\nu$ corresponds to the 5-50 μm (2000-200 cm^{-1}) region in the present investigation. Figure 1 shows the integrated radiance L as a function of θ for some climatological-average model atmospheres. Spectral flux M_ν can be obtained in principle by integrating $L_\nu(\theta)$ over the nadir angle $\theta(0-\pi/2)$ as

$$M_\nu = 2\pi\int_0^{\pi/2} L_\nu(\theta)\sin\theta\cos\theta\,\mathrm{d}\theta \qquad (3)$$

assuming azimuthal symmetry for infrared radiation.[6] In practice, however, lengthy numerical integration is avoided by using the diffusivity approximation.[7] Integrated flux M can be obtained by then integrating M_ν over the frequency range $\Delta\nu$, as in Eq. (2).

The spectral region 5-50 μm (2000-200 cm^{-1}) is divided into 180 narrow intervals, each 10 cm^{-1} wide. Atmospheric transmittance for each of these intervals was calculated using the quasirandom band model of absorption.[8] Spectral parameters of individual absorption lines for the computation were obtained from the AFCRL line parameters compilation.[9] It was shown by Tiwari and Gupta[10] that spectral transmittances of several infrared bands of atmospheric gases computed using this band model compared extremely well with their laboratory measured values. They also compared equally well with transmittances obtained using line-by-line integration while the computation cost for this model was approximately an order of magnitude smaller than with the line-by-line method. Continuum absorption by water vapor and its temperature dependence have been taken into account as outlined by Roberts et al.[11] For spectral region where bands of different constituents overlap, overall transmittances were obtained by multiplying the individual values. Height integration in the second term on the right-hand side of Eq. (1) is carried out up to 30 km.

The anisotropic function is defined as

$$R(\theta) = \pi L(\theta)/M \qquad (4)$$

Variation in $R(\theta)$ is shown for some climatological-average model atmospheres in Fig. 2. It decreases with increasing θ at a rate which is different for different atmospheric models. It can be seen from these curves that there is considerably more limb darkening in the tropical atmosphere than in the subarctic winter atmosphere. It was realized that the entire curve represents the same characteristic of a given atmospheric model and it was considered desirable to represent

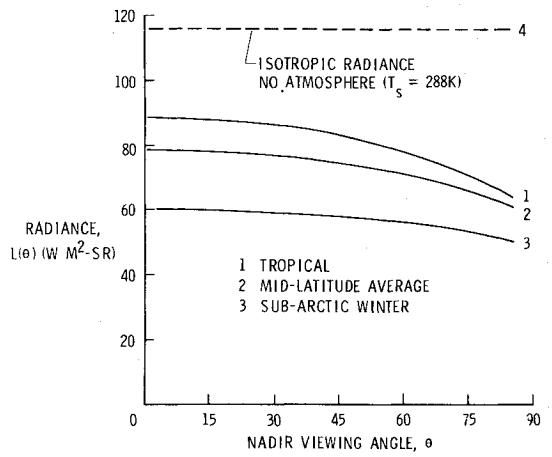

Fig. 1 Variation of upwelling radiance with nadir viewing angle for climatological-average model atmospheres.

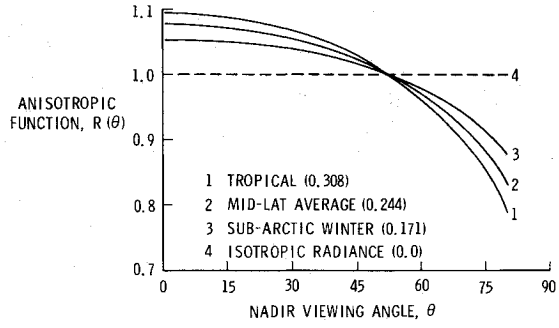

Fig. 2 Latitudinal variability of anisotropic functions for the climatological-average model atmospheres; numbers in parentheses represent the value of G.

the entire curve by a single parameter. The difference between the largest and smallest values of $R(\theta)$ is a good indicator of the extent of limb darkening for that atmospheric model. The desired parameter, which is characteristic of the atmospheric model, is defined, therefore, as

$$G = R(\theta_{\min}) - R(\theta_{\max}) \qquad (5)$$

This is because the largest value of $R(\theta)$ corresponds to the minimum value of θ and vice versa.

Meteorological Data

Several climatological-average model atmospheres have been used in the present study in order to establish the latitudinal and seasonal variability of the anisotropic functions. These were tropical, midlatitude summer/winter, and subarctic summer/winter, in addition to the U.S. Standard Atmosphere (USSA) which represents the mean-annual midlatitude conditions. Pressure, temperature, and ozone profiles for the models given earlier were taken from McClatchey et al.[12] A climatological mean value of 75% surface relative humidity[13] was adopted for all of the given models and vertical distribution of water vapor was computed using the power law[14]

$$w_z = w_z(p_z/p_s)^\lambda \qquad (6)$$

where λ is related to the water vapor scale height and its value equals 3. Sensitivity of the anisotropic functions to meteorological variables like cloud cover, cloud height, surface relative humidity, surface emittance, and temperature were examined for the USSA only.

Several radiosonde-measured atmospheric models were also used in the present study to further establish the latitudinal and seasonal variability of the anisotropic functions and to compare results for these models with those for the climatological-average models. These models were selected from a set of 106 radiosonde-measured models[15] covering all seasons and regions of the northern hemisphere, representing a very wide range of meteorological conditions.

Results and Discussion

Anisotropic functions, $R(\theta)$ for all model atmospheres discussed in the previous section were computed for seven different nadir viewing angles, namely, 0, 15, 30, 45, 60, 70, and 80 deg. Results for three climatological-average models, namely, tropical, midlatitude average (USSA), and subarctic winter are shown in Fig. 2. Values of G were, therefore, obtained as $[R(0)-R(80)]$ and are presented with the curves. The value of G for midlatitude average clear atmosphere was found to be 0.244 and is used as a reference value in the following discussion. The values for tropical and subarctic winter models were found to be 0.308 and 0.171, respectively. For comparison, the isotropic radiance case (no atmosphere) is represented by the dashed straight line and the corresponding value of G is zero. Similar latitudinal variability in anisotropic functions was observed when radiosonde-measured model atmospheres were used instead of the climatological-average models. Results from three of these models for Havana, Cuba (tropical), Nantucket, Mass. (midlatitude), and Thule, Greenland (subarctic) are shown in Fig. 3. Radiosonde measurements for all three of these locations were made on the same date and time (9/29/58; 1200 GMT) and the values of G for them were found to be 0.262, 0.220, and 0.165, respectively.

It should be noted that the differences between the anisotropic function curves for the different atmospheric models shown in Figs. 2 and 3 are small. Differences between various other models were found to be much smaller in most cases. It was difficult, therefore, to show many of these differences graphically even though they were significant. Such models were characterized entirely by their G values, all of which are presented in Table 1. Seasonal variability of the anisotropic functions and the parameter G was also investigated for the climatological-average as well as radiosonde-measured atmospheric models and these results are also presented in Table 1. Values of G in lines 3-6 represent its seasonal variability for midlatitude and subarctic models. Similar results for pairs of radiosonde-measured models representing three latitudinal regions are shown on lines 8-10.

Sensitivity of the anisotropic functions to changes in the values of various meteorological parameters was examined in detail only for the midlatitude average atmosphere and the results are presented in Table 2. Results for sensitivity to cloud cover were obtained for a cloud height of 6 km. It can be seen that G is quite sensitive to changes in fractional cloud cover varying from 0.244 for clear atmosphere to 0.128 for overcast condition. Sensitivity to cloud height was examined for overcast condition (100% cloud cover) and was found to be even greater as borne out by the results shown in Fig. 4. The value of G varies from 0.205 for $z_c = 2$ km to 0.014 for $z_c = 10$ km. Sensitivity of G to high-cloud ($z_c = 10$ km) emissivity was also examined and it was found that G varies from 0.014 for $\epsilon_c = 1.0$ to 0.162 for $\epsilon_c = 0.5$. Sensitivity to the variation of surface relative humidity at a fixed surface temperature was examined for a wide range of this variable. It was found that G increased sharply from 0.091 for a dry atmosphere (no water vapor) to 0.221 for 5% relative humidity, but increased very slowly thereafter. Results illustrating this variation are presented in Fig. 5. Variation of the scale-height parameter λ was also found to have a small effect on G. A 5-K change in surface temperature was found to have a moderate effect on G and so had the changes in surface emittance as shown in Table 2.

Table 1 Latitudinal and seasonal variability of anisotropic functions for climatological-average and radiosonde-measured atmospheric models

No.	Atmospheric model		G
1	Tropical annual average		0.308
2	Midlatitude average (USSA)		0.244
3	Midlatitude summer		0.259
4	Midlatitude winter		0.206
5	Subarctic summer		0.216
6	Subarctic winter		0.171
7	Havana, Cuba	9/29/58	0.262
	Nantucket, Mass.	9/29/58	0.220
	Thule, Greenland	9/29/58	0.165
8	Key West, Fla.	8/1/58	0.261
	Key West, Fla.	2/1/58	0.254
9	Grand Jn., Colo.	8/1/58	0.223
	Denver, Colo.	1/1/58	0.182
10	Eureka, NWT	8/1/58	0.166
	Eureka, NWT	3/1/58	0.117

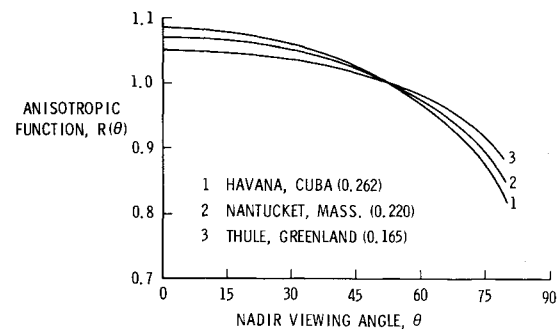

Fig. 3 Latitudinal variability of anisotropic functions for the radiosonde-measured atmospheric models.

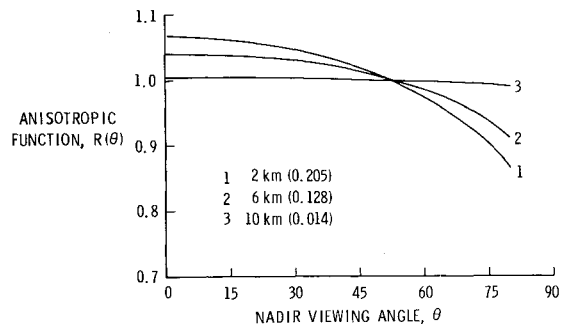

Fig. 4 Anisotropic functions for selected values of cloud-top height.

Several characteristics of the anisotropic functions become evident from the results of the sensitivity study presented in Table 2. Some of them help explain the latitudinal and seasonal variability of anisotropic functions observed with the climatological-average and radiosonde-measured atmospheric models presented in Table 1. The results for different values of relative humidity show that even though most of the limb darkening in the atmosphere is caused by the presence of water vapor, this effect reaches saturation for very low values of water vapor density. This is demonstrated by the fact that G increases sharply from the dry atmosphere to the 5% relative humidity model and increases very slowly thereafter.

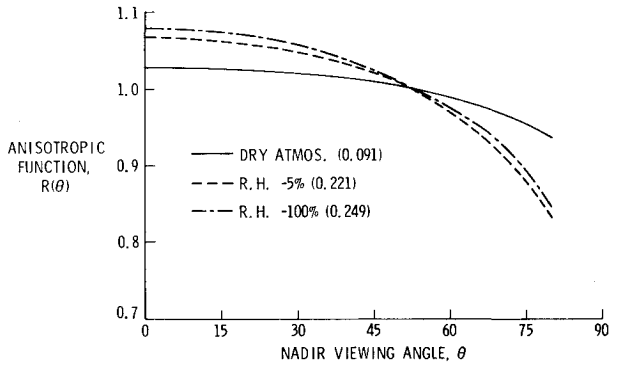

Fig. 5 Anisotropic functions for some values of surface relative humidity.

Table 2 Sensitivity of anisotropic functions to various meteorological parameters for a mean-annual midlatitude atmospheric model

No.	Meteorological parameter	G
1	Surface relative humidity, %	
	0	0.091
	5	0.221
	15	0.229
	25	0.232
	50	0.238
	75	0.244
	100	0.249
2	Water vapor scale-height parameter, λ	
	2	0.258
	3	0.244
	4	0.233
3	Surface temperature, K	
	283.15	0.227
	288.15	0.244
	293.15	0.260
4	Surface emittance	
	1.0	0.244
	0.9	0.223
	0.8	0.201
5	Cloud height (overcast), km	
	2	0.205
	6	0.128
	10	0.014
6	Cloud cover ($z_c = 6$ km)	
	Clear	0.244
	Partly cloudy (50%)	0.195
	Overcast	0.128
7	High-cloud emissivity	
	1.0	0.014
	0.5	0.162

Model results were also obtained to determine the effect of varying carbon dioxide concentration. It was found that (results not shown in Table 2) variation of carbon dioxide concentration between zero and 2 × standard (i.e., 660 ppmV) has a very small effect on G.

A 5-K change in surface temperature without changing the atmospheric temperature profile was found to cause more than 6% change in G and, as shown in Table 2, a 10% change in surface emittance has an even larger effect. It should be noted that the preceding changes of surface temperature and emittance effectively amount to a change in the lapse rate, to which these changes of G may be attributed. When atmospheric-temperature profile was changed along with the surface temperature, insignificant changes in G were observed. It can be inferred, therefore, that most of the latitudinal and seasonal variability of G in clear atmospheres, as seen in the results presented in Table 1, is due to changes in the lapse rate and, to a smaller extent, due to variability of the water vapor content.

The strong dependence of G on cloud height as shown in Table 2 is a combination of two effects. First, the lower temperature of the cloud top reduces the temperature difference between the underlying surface (cloud top) and top layers of the atmosphere. Second, there is much less water vapor above the cloud top. Variation of G with fractional cloud cover is simply a combination of the effects for clear and overcast cases. The large increase in G as the high-cloud emissivity decreases from 1.0 to 0.5 can be attributed to the fact that for the partly transmitting cloud, considerable part of the radiation emanating at the top originated at the surface. It should be noted that the values of G for 50% cloud cover and $\epsilon_c = 1.0$ is equal to that for 100% cloud cover and $\epsilon_c = 0.5$, which demonstrates the cloud emissivity and fractional cloud cover are equivalent parameters, i.e., the effective cloud cover is $\epsilon_c \times$ actual cloud cover.

Recently,[16] the entire study has been extended to cover the longwave spectral range 5-200 μ and extensive results have been obtained for different atmospheric models and climatological parameters. The results show that inclusion of the spectral range from 50 μ to 200 μ amounts to about 3% change in final results in most cases.

Concluding Remarks

Studies conducted with an accurate radiative transfer model show considerable latitudinal and seasonal variation of the anisotropic functions for the Earth-atmosphere system. It is established that limb darkening in the atmosphere is caused primarily by the presence of water vapor and reaches saturation for very low values of water vapor burden. As a result, while G increases sharply for a relative humidity increase from 0 to 5%, no significant change in G is observed for an increase from 25 to 100%. Doubling of carbon dioxide or excluding it altogether also shows an insignificant effect on G. Changes of surface temperature and emittance which amount to a change of lapse rate show a considerably larger effect on the anisotropic functions. Cloud height exhibits a strong effect on the anisotropic functions; firstly, because a great bulk of atmospheric water vapor is located below the clouds and, secondly, the lower cloud top temperature drastically reduces the temperature difference between the underlying surface and the top of the atmosphere. Changes in fractional cloud cover and cloud emissivity have equivalent effects on anisotropic functions as the effective cloud cover is ϵ_c times the actual cloud cover.

Acknowledgment

The authors wish to express their gratitude to Dr. Bruce A. Wielicki of the NASA Langley Research Center for his critical review of the manuscript and many valuable suggestions.

References

[1] Vonder Haar, T. H. and Soumi, V. E., "Measurement of the Earth's Radiation Budget from Satellites During a Five-Year Period, 1. Extended Time and Space Means," *Journal of the Atmospheric Sciences*, Vol. 28, 1971, pp. 305-314.

[2] Smith, W. L., Hickey, J., Howell, H. B., Jacobowitz, H., Hilleary, D. T., and Drummond, A. J., "Nimbus 6 Earth Radiation Budget Experiment," *Applied Optics*, Vol. 16, 1977, pp. 306-318.

[3] Vonder Haar, T. H. and Smith, G. L. (eds.), "Earth Radiation Budget Science, 1978," NASA CP-2100, 1979.

[4] Wark, D. Q., Yamamoto, G., and Lienesch, J. H., "Methods of Estimating Infrared Flux and Surface Temperature from Meteorological Satellites," *Journal of the Atmospheric Sciences*, Vol. 19, 1962, pp. 369-384.

[5] Raschke, E., Vonder Haar, T. H., Pasternak, M., and Bandeen, W. R., "The Radiation Balance of the Earth-Atmosphere System from Nimbus-3 Radiation Measurements," NASA TN D-7249, 1973.

[6] Paltridge, G. W. and Platt, C. M. R., *Radiative Processes in Meteorology and Climatology*, Elsevier Scientific Publishing Co., Amsterdam, the Netherlands, 1976.

[7] Rodgers, C. D. and Walshaw, C. D., "The Computation of Infrared Cooling Rate in Planetary Atmospheres," *Quarterly Journal of the Royal Meteorological Society*, Vol. 92, 1966, pp. 67-92.

[8] Wyatt, P. J., Stull, V. R., and Plass, G. N., "Quasi-Random Model of Band Absorption," *Journal of the Optical Society of America*, Vol. 52, 1962, pp. 1209-1217.

[9] McClatchey, R. A. et al., "AFCRL Atmospheric Absorption Line Parameters Compilation," AFCRL-TR-73-0096, 1973.

[10] Tiwari, S. N. and Gupta, S. K., "Accurate Spectral Modeling for Infrared Radiation," *Journal of Heat Transfer*, Vol. 100, 1978, pp. 240-246.

[11] Roberts, R. E., Selby, J. E. A., and Biberman, L. M., "Infrared Continuum Absorption by Atmospheric Water Vapor in the 8-12 μm Window," *Applied Optics*, Vol. 15, 1976, pp. 2085-2090.

[12] McClatchey, R. A., Fenn, R. W., Selby, J. E. A., Volz, F. E., and Garing, J. S., "Optical Properties of the Atmosphere," AFCRL-72-0497, 1972.

[13] Manabe, S. and Wetherald, R. T., "Thermal Equilibrium of the Atmosphere with a Given Distribution of Relative Humidity," *Journal of the Atmospheric Sciences*, Vol. 24, 1967, pp. 241-259.

[14] Smith, W. L., "Note on the Relationship Between Total Precipitable Water and Surface Dew Point," *Journal of Applied Meteorology*, Vol. 5, 1966, pp. 726-727.

[15] Wark, D. Q., Yamamoto, G., and Lienesch, J. H., "Infrared Flux and Surface Temperature Determinations from Tiros Radiometer Measurements," NOAA Meteorological Satellite Laboratory, Rept. 10, 1962.

[16] Tiwari, S. N., Vemuru, C. S., and Subramanian, S. V., "Analysis of Longwave Radiation for the Earth-Atmosphere System," School of Engineering Old Dominion University, Norfolk, Va., Tech. Rept. NAG-1-21, Nov. 1983.